Effects of Channel Cytoplasmic Regions on the Activation Mechanisms of Cardiac versus Skeletal Muscle Na$^+$ Channels

Eric S. Bennett

Department of Physiology and Biophysics, College of Medicine, University of South Florida, Tampa, Florida 33612 USA

ABSTRACT   Functional comparison of skeletal muscle (rSkM1) and cardiac (hH1) voltage-gated sodium channel isoforms expressed in Chinese hamster ovary cells showed rSkM1 half-activation (V_a) and inactivation (V_i) voltages 7 and 10 mV more depolarized than hH1 V_a and V_i, respectively. Internal papain perfusion removed fast inactivation from each isoform and caused a 20-mV hyperpolarizing shift in hH1 V_a, with an insignificant change in rSkM1 V_a. Activation voltage of the inactivation-deficient hH1 mutant, hH1Q3, was nearly identical to wild-type hH1 V_a, both before and after papain treatment, with hH1Q3 V_a also shifted by nearly 20 mV after internal papain perfusion. These data indicate that while papain removes both hH1 and rSkM1 inactivation, it has a second effect only on hH1 that causes a shift in activation voltage. Internal treatment with an antibody directed against the III-IV linker essentially mimicked papain treatment by removing some inactivation from each isoform and causing a 12-mV shift in hH1 V_a, while rSkM1 V_a remained constant. This suggests that some channel segment within, near, or interacting with the III-IV linker is involved in establishing hH1 activation voltage. Together the data show that rSkM1 and hH1 activation mechanisms are different and are the first to suggest a role for a cytoplasmic structure in the voltage-dependent activation of cardiac sodium channels.

INTRODUCTION

Voltage-gated sodium channels are responsible for the initiation and propagation of nerve, skeletal muscle, and cardiac action potentials. The orchestrated activation and inactivation gating of sodium channels is vital to normal neuronal signaling, skeletal muscle contraction, and normal heart rhythms. Voltage-gated sodium channels as well as many other ion channels are molecularly diverse, with different channel isoforms expressed specifically by cell type or throughout development (for reviews see Kallen et al., 1993; Catterall, 1995; Jan and Jan, 1997). Often several isoforms are expressed within a single cell. To date, at least nine different sodium channel α subunit isoforms from a single species have been isolated and cloned. What is the need for this diversity of channels? What are the functional differences among these isoforms, and how are these differences relevant to the cell type and/or developmental stage in which the channel is expressed?

These questions as well as basic questions relating channel structure to function can be addressed through stable and transient expression of ion channels in mammalian and amphibian heterologous expression systems. Comparison of mutant versus wild-type channel function expressed in heterologous systems has provided significant insight into the functionally relevant regions of ion channels (see, e.g., Stuhmer et al., 1989; Ukomadu et al., 1992; West et al., 1992). In addition, functional differences among isoforms

of a given ion channel species can be observed through parallel experimentation in a single cellular system.

Previous reports compared function of the skeletal muscle sodium channel isoforms SkM1 and SkM2 (H1) transiently expressed in *Xenopus* oocytes and in a human embryonic kidney (HEK)-derived cell line, tsA201 (Chen et al., 1992; Chahine et al., 1996; Wang et al., 1996; Richmond et al., 1998). These two isoforms are expressed natively in adult (SkM1) and embryonic (SkM2; also denervated) skeletal muscle, respectively (Trimmer et al., 1990; Yang et al., 1991; Gellens et al., 1992; Kallen et al., 1993). The H1 isoform is the predominant channel isoform expressed in the heart and is identical to SkM2 (Rogart et al., 1990; Gellens et al., 1992).

Here functional comparison of rSkM1 and hH1 in a Chinese hamster ovary (CHO) cell line, CHO-K1, reveals a novel difference in function between the two isoforms. While internal papain treatment removes both rSkM1 and hH1 inactivation, the half-activation voltage (V_a) for hH1 is also shifted dramatically in the hyperpolarized direction with little or no impact on rSkM1 V_a. The data are consistent with a major difference between hH1 and rSkM1 in their voltage dependence of activation, indicating that hH1 activation can be altered through cytoplasmic channel structures. The possibility that the kinetic uncoupling of inactivation from activation is responsible for this shift in V_a is ruled out through studies of the inactivation-deficient mutant hH1Q3, in which hH1Q3 V_a closely follows hH1 V_a. In the mutant, hH1Q3, the IFM consensus inactivation sequence (a.a. 1484–1486) was replaced with three glutamine residues to remove fast inactivation (see Hartmann et al., 1994). This is investigated further by comparing hH1 and rSkM1 function before and after treatment with an affinity-purified antibody directed against the putative inactivation loop (III-IV linker). These data are similar to those observed

after papain treatment, indicating some type of interaction between the heart channel isoform III-IV linker (but not the IFM consensus inactivation sequence directly) and the activation mechanism. Because rSkM1 activation is not altered by such treatment, rSkM1 is missing this sequence or it is differently linked to channel activation. These data imply that cytoplasmic structural differences between cardiac and skeletal muscle sodium channel isoforms exist that have direct and different impacts on channel activation, and they are the first examples to indicate that cytoplasmic structures affect voltage-dependent cardiac channel activation.

MATERIALS AND METHODS

CHO cell transfection and tissue culture methods

CHO cells were transfected with the plasmid rSkM1-pZem (Bennett et al., 1997; rSkM1 first isolated and cloned by Trimmer et al., 1989) or hH1-CMV (a generous gift of R. G. Kallen; first isolated and cloned by Gellens et al., 1992) via a calcium phosphate-mediated technique using 20 μg DNA and 5×10^5 cells in 10 ml of Dulbecco's minimum essential medium-fetal bovine serum as described previously (Bennett et al., 1997). After 24 h of incubation with DNA, standard culturing conditions were resumed. After 3 days, stably transfected cells were selected with 500 μg/ml Geneticin (G418; GIBCO). Transfected cells were grown to confluence (~3 weeks) and then passaged.

The experiments shown in Fig. 7 compare the function of hH1 and that of the inactivation-deficient mutant, hH1Q3 (a generous gift of Dr. H. Hartmann). In the mutant hH1Q3, the IFM consensus inactivation sequence (a.a. 1484–1486) was replaced with three glutamine residues (see Hartmann et al., 1994). hH1 and hH1Q3 expression vectors were transfected into CHO cells by liposomal technologies. Briefly, CHO cells were passaged onto 35-mm culture plates at ~40% confluence. After a 24-h incubation, cells were then exposed to a 1-ml Opti-MEM (GIBCO Life Technologies) medium containing 8 μl lipofectamine (GIBCO) and 1–2 μg DNA, consisting of ~12% pGreen Lantern-1 (GFP; GIBCO) and ~88% either hH1 or hH1Q3 expression vector. After a 5-h incubation at 37°C in a 5% CO_2 humidified incubator, the medium was exchanged for normal, nonselective CHO cell growing medium. Cells were incubated for 60–72 h before electrophysiological recordings, selecting cells expressing GFP.

Controls were conducted to ensure that channel function in transient transfectants was not different from channel activity in stably transfected CHO cells. Transient transfectants showed typical activation voltages, reversal potentials, current levels, kinetics, etc., indicating no significant difference in channel function between stable and transient transfectants. For example, transient hH1 V_a measured -30.4 ± 2.9 mV ($n = 3$), while stable hH1 V_a was -28.6 ± 1.8 mV ($n = 7$). In addition, as shown in Fig. 1 below for the stable transfectants, neither hH1 nor hH1Q3 transient transfectants showed any drift in voltage-dependent gating over time ($n > 5$ for each channel type).

Antibody production and purification

Site-directed polyclonal antibodies (α1Abs) were raised to an 18-mer peptide (pep-α1; α Diagnostics) corresponding to the highly conserved III-IV linker region (TEEQKKYYNAMKKLGSKK) in vertebrate sodium channels and were affinity-purified on a pep-α1-coupled column. Antibody concentrations were assayed using optical density (O.D.) measurements at a 280-nm wavelength, with the accepted estimate that a 1.0 O.D. reading approximates 0.8 mg/ml α1Ab (Harlow and Lane, 1988).

Whole-cell recording of sodium currents in CHO cells

CHO cells were studied using the patch-clamp whole-cell recording technique described previously (Bennett et al., 1997). Cells were passaged and plated on 35-mm culture dishes 24–96 h before the experiment.

An Axon Instruments 200B patch-clamp amplifier with a CV203BU headstage (Axon Instruments) was used in combination with a Nikon TE300 inverted microscope. Pulse protocols were generated using a 200-MHz Pentium II computer (Dell Computers) running Pulse acquisition software (HEKA). The resultant analog signals were filtered at 5 kHz (50 kHz for the kinetic studies), using an eight-pole Bessel filter (9200 LPF; Frequency Devices) and then digitized using the ITC-16 AD/DA converter (Instrutech).

Narishige micromanipulators (both mechanical and hydraulic) were used to place the electrode on the cell. Electrode glass (Drummond capillary tubes, 2-000-210) was pulled using a two-step process on a Sutter (model P-87) electrode puller to a resistance of 1–2 MΩ measured in the salt solutions used. Two different sets of solutions were used, solution set A (Fig. 1, A–C) and solution set B (Figs. 1 D through 9). External solution A was (in mM) 134 NaCl, 4 KCl, 1.5 CaCl$_2$, 1.5 MgCl$_2$, 5 glucose, and 5 HEPES, and internal solution A was (in mM) 90 CsF, 60 CsCl, 11 NaCl, and 5 HEPES. (Both solutions were titrated with 1 N NaOH to pH 7.4 at room temperature.) External solution B was (in mM) 224 sucrose, 22.5 NaCl, 4 KCl, 2.0 CaCl$_2$, 5 glucose, and 5 HEPES, and internal solution B was (in mM) 120 sucrose, 60 CsF, 32.5 NaCl, and 5 HEPES (titrated with 1 N NaOH to pH 7.4 at room temperature). Please note the low ionic strength of solution set B. Currents measured using these solutions are approximately one-fourth the magnitude of currents measured using set A solutions. Although series resistance was compensated 95–98% for all data, the smaller current produced using set B solutions further minimized any remaining series resistance error. All solutions were filtered using Gelman 0.2-μm filters immediately before use. All experiments were carried out at room temperature (21–23°C).

Pulse protocols

Conductance-voltage (G-V) relationship

The cell was held at -100 mV, stepped to various depolarized potentials (ranging from -60 (or -80) to $+100$ mV in 10-mV increments) for 10 ms, and then returned to the holding potential. Consecutive pulses were stepped every 1.5 s, and the data were leak subtracted using the P/4 method, stepped negatively from the -100 mV holding potential. At each test potential, steady-state whole-cell conductance was determined by measuring the peak current at that potential and dividing by the driving force (i.e., difference between the membrane potential and the observed reversal potential). The maximum conductance generated by each cell was used to normalize the data for each cell to its maximum conductance by fitting the data to a single Boltzmann distribution (Eq. 1). The average $V_a \pm$ SEM values listed throughout are determined from these single Boltzmann distributions. The normalized data were then averaged with those from other cells, and the resultant average conductance-voltage curve was fit via least squares, using the following Boltzmann relation:

Fraction of maximal conductance

$$= [1 + \exp - ((V - V_a)/K_a)]^{-1}, \qquad (1)$$

where V is the membrane potential, V_a is the voltage of half-activation, and K_a is the slope factor.

Steady-state inactivation curves (h_{int})

The voltage dependence of steady-state inactivation was determined by first prepulsing the membrane for 500 ms from the -100 mV holding potential, then stepping to $+60$ mV for 5 ms, and then returning to the

−100-mV holding potential. The prepulse voltages ranged from −130 mV to +10 mV in 10-mV increments. The currents from each cell were normalized to the maximum current. The normalized data for many cells were then averaged and fit to Eq. 2, from which the mean V_i and slope factor (K_i) parameters describing steady-state inactivation for the channel population were calculated:

$$\text{Fraction of maximum current} = [1 + \exp((V - V_i)/K_i)]^{-1}. \tag{2}$$

Recovery from inactivation

Cells were held at −100 mV, then stepped to +60 mV for 10 ms and returned to the recovery potential for a varying duration ranging from 1 to 20 ms in 1-ms increments. After this recovery pulse, the potential was again stepped to +60 mV for 10 ms. The peak currents measured during the two +60-mV depolarizations were compared, and the fractional peak current remaining during the second depolarization was plotted as a function of the recovery pulse duration. This represents the percentage of channels that recovered from inactivation during the recovery interval. Time constants of recovery were determined by fitting the data to single-exponential functions.

Measurement of gating kinetics

Sodium channel inactivation was removed to measure directly the time constants of channel activation and deactivation. Before inactivation removal, normal current traces were obtained for later extraction of inactivation time constants. Cells were internally perfused with papain (1 mg/ml Type X; Sigma) as described (Bennett et al., 1997); removal of inactivation occurred within 15 min.

To determine deactivation time constants, channels were fully activated after papain treatment with a pulse to +60 mV for 1.0 ms, and deactivation currents were elicited by hyperpolarizing pulses from −80 to −30 mV (−50 mV for hH1) for 10 ms. Deactivation time constants were obtained by fitting the resultant currents to a single-exponential decay.

Activation time constants were calculated for potentials ranging from −60 mV (−50 mV for rSkM1) to +20 mV, using the standard activation protocol (above) and fitting the rise of current (in the absence of inactivation) to the steady state, using a fourth-power exponential function (Oxford, 1981) as follows:

$$y = y_0(1 - \exp(-t/\tau_m))^4, \tag{3}$$

where y_0 is the peak current at the test potential, t is the time after the pulse onset, and τ_m is the activation time constant. Fits of the data using exponential functions raised to various powers indicated that the fourth-power exponential fit the data best.

Inactivation time constants were determined by fitting the current traces obtained from the same cell before removal of inactivation. Attenuating currents from 90% to 10% of the peak values were fit to a single-exponential function. All currents were analog filtered at 50 kHz before digitization to improve time resolution.

Internal perfusion of α1Ab and pep-α1

The purified antibody, α1Ab, was added to internal solution B to a final concentration of 80 μg/ml. The blocking peptide, pep-α1, was added to this solution at a concentration of 80 μg/ml.

Data analysis

The data were analyzed using a combination of Pulse/PulseFit (HEKA) and SigmaPlot 4.0 (Jandel Scientific) software.
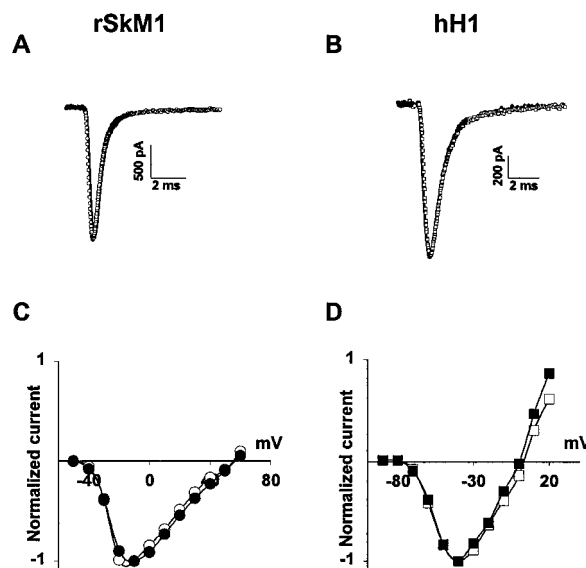

FIGURE 1   There is no time-dependent shift in activation voltage. (*A*) CHOM1 current trace during a −10 mV test potential at 5 (——) and 14 (○) min after WCR. (*B*) CHOH1 current trace during a 0-mV test potential at 5 (——) and 16 (□) min after WCR. (*C*) Current-voltage (*I-V*) relationship for a CHOM1 cell measured at two times after WCR. Points are peak currents measured at 5 (○) and 33 (●) min after WCR. (*D*) *I-V* relationship for a CHOH1 cell measured at two times after WCR. Points are peak currents measured at 5 (□) and 25 (■) min after WCR.

RESULTS

rSkM1 and hH1 activation voltages are stable as expressed in CHO cells

Whole-cell currents were recorded from CHO-K1 cells transfected with rSkM1 (CHOM1) and hH1 (CHOH1). Peak sodium currents of 0.5–8 nA were recorded in most transfected cells and showed rapid activation and inactivation, reversing at potentials consistent with those predicted by the Na$^+$ concentration gradients. Current traces with similar characteristics were observed using either solution set A or solution set B. Peak currents measured in set A solutions were about four times those measured in set B solutions, consistent with the predicted impact of the lowered ionic strength of set B solutions. There was no detectable decrease in sodium channel expression with subsequent passaging, indicating stable expression of rSkM1 and hH1 in CHO cells.

Throughout this study, data were collected at times from 5 to 30 min after attainment of the whole-cell configuration (WCR). Most experiments were completed within 15–20 min. Previous reports studying sodium channel function in tsA201 cells indicated that the voltage of activation drifted in the hyperpolarizing direction over time (Chahine et al., 1996; Wang et al., 1996). Wang et al. (1996) showed that the voltage of half-activation (V_a) for hSkM1 shifted by ~25 mV in the hyperpolarized direction within 60 min after WCR, while hH1 showed a smaller shift that stabilized within 20 min.

There is no sign of such a drift in voltage dependence over time (starting 5 min post-WCR) for rSkM1 or for hH1 as expressed in CHO cells. Fig. 1 shows typical current traces for a CHOM1 (Fig. 1 *A*) and a CHOH1 (Fig. 1 *B*) cell at 5 and ~15 min after WCR. Note that there is no difference between the current traces over time. Furthermore, Fig. 1 shows the current-voltage relationships for another CHOM1 (Fig. 1 *C*) and a CHOH1 (Fig. 1 *D*) cell at 5 and 25–33 min after WCR. Note that neither rSkM1 nor hH1 shows any significant drift in voltage dependence with time. These experiments were repeated many times in both solution sets and for hH1 and hH1Q3 transient transfectants, with no indication of any significant drift in activation voltage over time ($n > 25$). Thus, for the time course of experiments used throughout this study, there is no drift in gating voltage dependence.

rSkM1 versus hH1: comparison of steady-state parameters

Fig. 2 *A* shows the conductance-voltage curve comparing rSkM1 and hH1 steady-state activation as expressed in CHO cells. hH1 activates at potentials 7 mV more hyperpolarized than does rSkM1, with $V_a = -21.8 \pm 2.6$ mV ($n = 8$) and -28.6 ± 1.8 mV ($n = 7$) for rSkM1 and hH1, respectively.

Fig. 2 *B* shows the h_{inf} curve for rSkM1 versus hH1 and indicates that hH1 inactivates at potentials 10 mV more hyperpolarized than rSkM1, with $V_i = -59.4 \pm 3.2$ mV ($n = 10$) and -69.4 ± 2.9 mV ($n = 7$) for rSkM1 and hH1, respectively.

Recovery from inactivation: rSKM1 recovers more quickly than hH1

Fig. 3 *A* shows the rate of recovery from inactivation for each isoform. Note that rSkM1 recovers from inactivation more rapidly than hH1. At a -120-mV recovery potential, the recovery time constant (τ) was 1.1 ± 0.1 ms ($n = 7$) for rSkM1 and τ was 2.1 ± 0.1 ms ($n = 5$) for hH1. Recovery from inactivation was complete in these cells, with no indication of a second, slower rate to recovery.

Fig. 3 *B* plots the potential dependence of the recovery rates and shows that the two isoforms, while recovering from inactivation with inherently different rates, show similar potential dependencies. These data indicate that that the absolute rate of recovery from inactivation distinguishes the isoforms and not the relative potential dependence of the recovery mechanism. Recovery time constants increased *e*-fold every 24 and 29 mV for hH1 and rSkM1, respectively. These values are in close agreement with previous reports for other sodium channel isoforms (Keynes, 1986; Patlak, 1991).

Gating kinetics for rSkM1 versus hH1

Fig. 4 *A* plots the time constants of activation and deactivation for rSkM1 versus hH1 and shows that hH1, at the
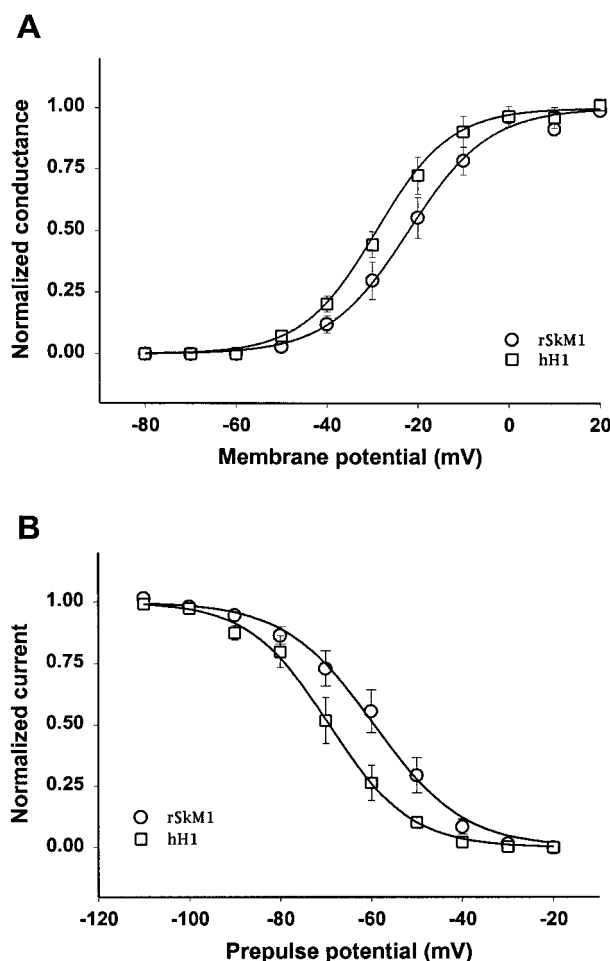

FIGURE 2   Comparison of rSkM1 and hH1 steady-state gating parameters. (*A*) Conductance-voltage (*G-V*) relationship. Data are the average normalized peak conductance $\pm$ SEM at a membrane potential. Curves are fits of the data to single Boltzmann distributions. $\bigcirc$, rSkM1; $\square$, hH1. Average voltages of activation (V_a) = -21.8 ± 2.6 mV (rSkM1; $n = 8$); $-28.6* \pm 1.8$ mV (hH1; $n = 7$). Significance was tested throughout using a two-tailed test, demarcating significance as follows: *, $p < 0.05$; **, $p < 0.01$; #, not significant ($p > 0.05$). (*B*) Steady-state inactivation (h_{inf}). Data are the average normalized current $\pm$ SEM measured during a 5-ms pulse to $+60$ mV after a 500-ms prepulse to the plotted potentials. Curves are fits of the data to single Boltzmann distributions. $\bigcirc$, rSkM1; $\square$, hH1. Average voltages of half-inactivation (V_i) = -59.4 ± 3.2 mV (rSkM1; $n = 10$); $-69.4* \pm 2.9$ mV (hH1; $n = 7$).

activating potentials ranging from -50 to $+20$ mV, activates more rapidly than rSkM1, consistent with the relative potential dependence of steady-state activation (see the *G-V* curves of Fig. 5, *C* and *D*, following papain treatment).

Fig. 4 *B* shows the time constants of inactivation and indicates that hH1 inactivates slightly faster than rSkM1 at small depolarizations. The rates of inactivation for the two isoforms converge at larger depolarizations. The percentage of a second, slower inactivation rate, calculated by fitting the offset of current to a double-exponential function, was minimal for each isoform, with hH1 showing an average $7.1 \pm 1.2\%$ ($n = 30$) slower inactivation versus $7.7 \pm 1.1\%$ ($n = 61$) for rSkM1.
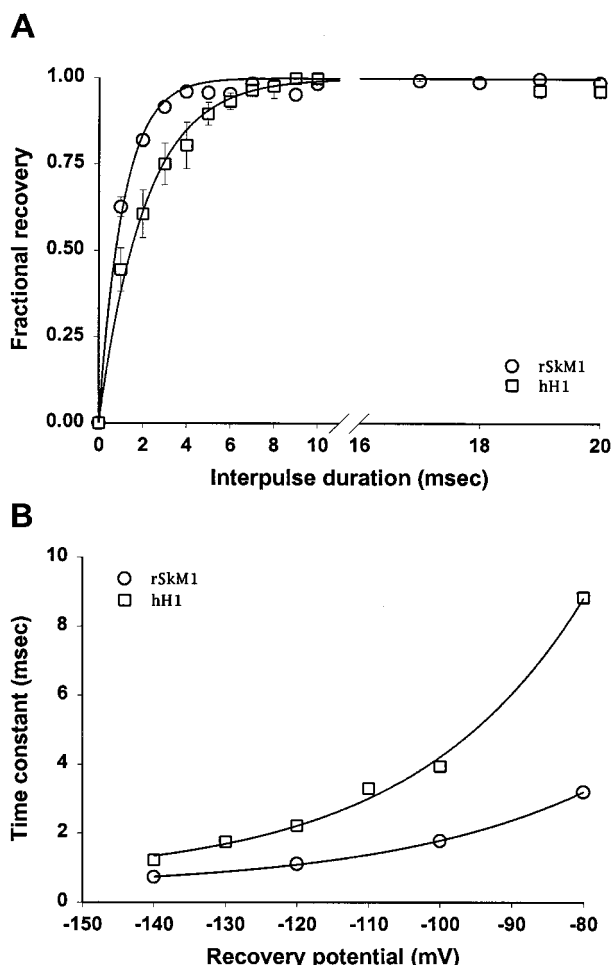
A

B

FIGURE 3 Recovery from inactivation is relatively rapid for both isoforms. (*A*) Recovery from inactivation at a −120 mV recovery potential. Data represent the average fractional current measured as described, after a −120 mV recovery potential of varied duration. Curves are fits of the data to single exponential functions. ○, rSkM1; □, hH1. Time constants (τ): $\tau_{\text{rSkM1}} = 1.1 \pm 0.06$ ms ($n = 7$); $\tau_{\text{hH1}} = 2.1^{**} \pm 0.1$ ms ($n = 5$). (*B*) Potential dependence of recovery time. Data are the time constants of recovery, measured as in *A* at different recovery potentials (○, rSkM1; □, hH1; $n = 5$–7 for each point). Curves are fits of the data to a single exponential function and indicate an *e*-fold increase in τ_{hH1} and τ_{rSkM1} every 24-mV and 29-mV depolarization, respectively.

Internal papain removes inactivation from rSkM1 and from hH1—a large shift in hH1 activation voltage is also observed, with little effect on rSkM1 V_a

To determine accurately the rates of activation and inactivation, the gating processes must be separated. As such, sodium channel inactivation was removed through internal papain perfusion, and the gating time constants shown in Fig. 4 were measured. Fig. 5, *A* and *B*, shows current traces from CHOM1 and CHOH1 cells before and after complete removal of inactivation, respectively. Whole-cell currents were smaller after papain treatment, with relative peak conductances of $71.9 \pm 10.0\%$ ($n = 8$) and $71.1 \pm 8.8\%$ ($n = 7$) of control peak conductance for rSkM1 and hH1, respectively.
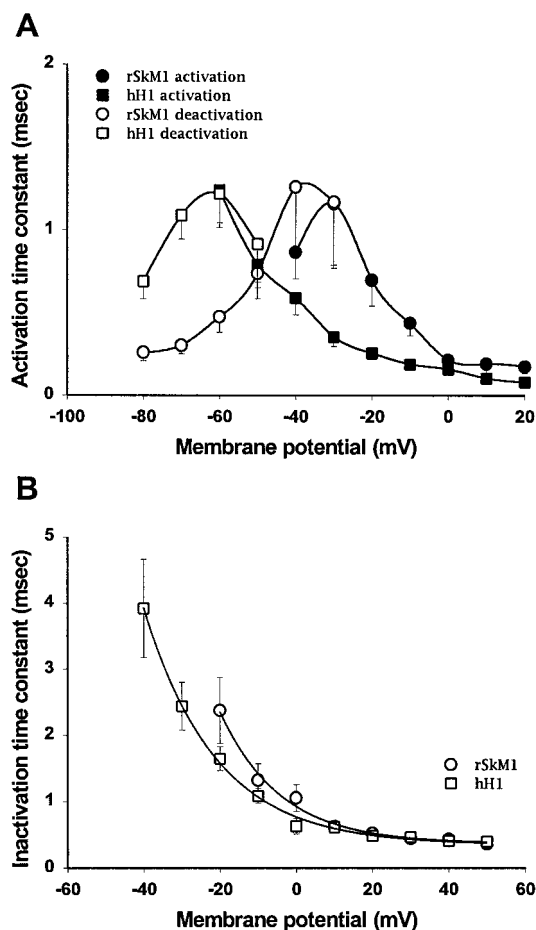
A

B

FIGURE 4 Comparison of rSkM1 and hH1 activation and inactivation rates. (*A*) Time constants of activation and of deactivation. Data are the average time constants $\pm$ SEM after the removal of inactivation and determined as described in Materials and Methods. Curves are nontheoretical point to point. ●, rSkM1 activation ($n = 5$); ○, rSkM1 deactivation ($n = 5$); ■, hH1 activation ($n = 4$); □, hH1 deactivation ($n = 4$). (*B*) Time constants of inactivation. Data are the average time constants of inactivation $\pm$ SEM measured as described in Materials and Methods. Curves are nontheoretical, point to point. ○, rSkM1 ($n = 7$); □, hH1 ($n = 7$).

A notable difference in channel gating between the two isoforms was observed after papain treatment. Fig. 5 shows the average *G-V* relationships for rSkM1 (Fig. 5 *C*) and hH1 (Fig. 5 *D*) before and after removal of inactivation. Note that rSkM1 V_a is only slightly (insignificantly) affected by papain treatment, while hH1 V_a shifts by more than 20 mV in the hyperpolarized direction after papain treatment. This phenomenon was observed for all CHOH1 cells tested, with hyperpolarizing shifts in V_a ranging from 13 to 29 mV, averaging 20.7 ± 1.9 mV ($n = 7$).

The time to peak current for hH1 does not change when inactivation is removed

Previous reports have described channel activity after the removal of inactivation through enzyme treatment and/or chemical modification (Armstrong and Bezanilla, 1973, 1977; Eaton et al., 1978; Oxford et al., 1978; Horn et al.,
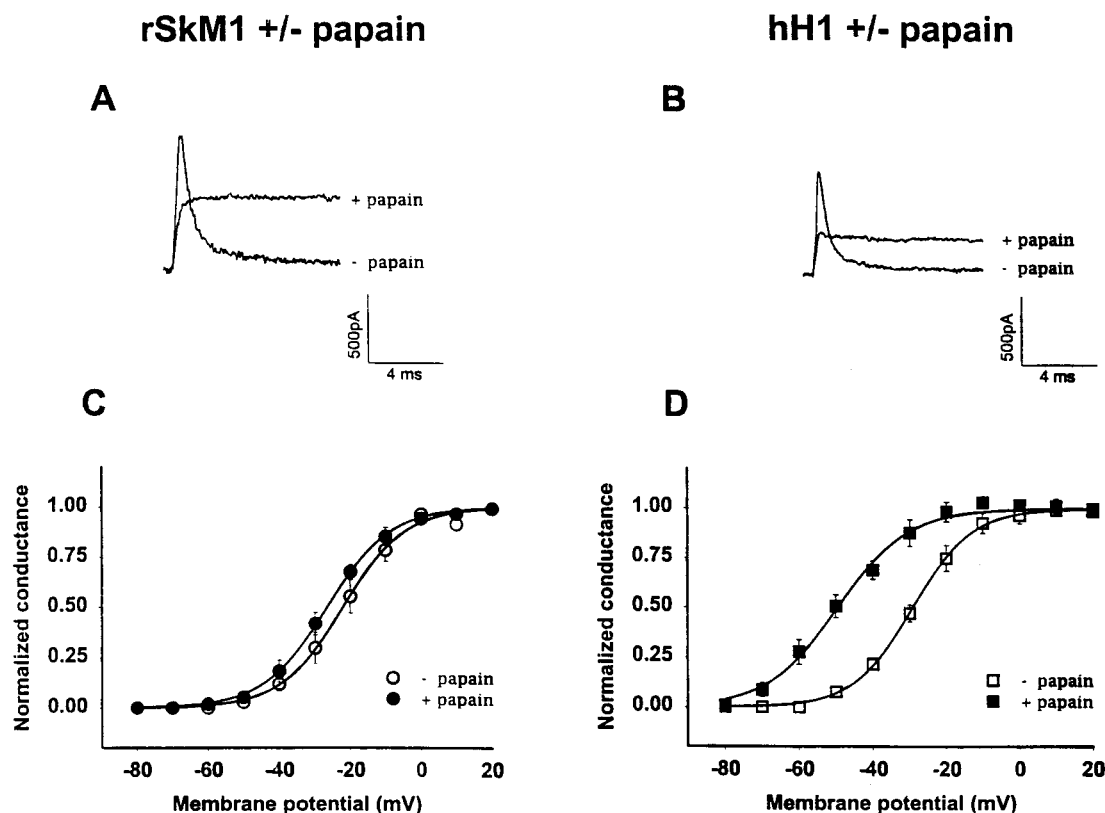
rSkM1 +/- papain

A

hH1 +/- papain

B

C

D

FIGURE 5 Papain removes rSkM1 and hH1 inactivation but causes a shift only in hH1 activation voltage. (*A*) Whole-cell current trace from a typical CHOM1 cell to a +30-mV test potential before and after the removal of inactivation through internal papain treatment. (*B*) Whole-cell current trace from a typical CHOH1 cell to a +30-mV test potential before and after the removal of inactivation through internal papain treatment. (*C*) *G-V* relationship for rSkM1 before and after papain treatment. Data are the average normalized peak conductance $\pm$ SEM at a membrane potential. Curves are fits of the data to single Boltzmann relationships. $\bigcirc$, Inactivation present; $V_a = -21.8 \pm 2.6$ mV. $\bullet$, Inactivation removed; $V_a = -26.8^{\#} \pm 2.2$ mV. $n = 8$ for each set. (*D*) *G-V* relationship for hH1 before and after papain treatment. Data are the average normalized peak conductance $\pm$ SEM at a membrane potential. Curves are fits of the data to single Boltzmann relationships. $\square$, Inactivation present; $V_a = -28.6 \pm 1.8$ mV. $\blacksquare$, Inactivation removed; $V_a = -49.3^{**} \pm 2.5$ mV. $n = 7$ for each set.

1980; Oxford, 1981; Stimers et al., 1985; Gonoi and Hille, 1987; Kirsch et al., 1989). In most tissues, investigators have found results similar to those observed here for rSkM1. That is, removal of fast inactivation, regardless of the method, had a measurable impact on only two aspects of channel function: inactivation was removed in all cases, and the current magnitude may have been reduced. The voltage dependence of activation was essentially unaltered.

One set of notable exceptions to these findings was shown for sodium channel function in neuroblastoma cell lines (Gonoi and Hille, 1987; Kirsch et al., 1989). Gonoi and Hille reported a 25-mV hyperpolarizing shift in V_a after removal of inactivation with several different chemical modifiers. The authors concluded that activation voltages shift because of the uncoupling of fast inactivation from slow activation at small depolarizations. When inactivation is removed, the channels, while activating at lesser depolarizations, do so relatively slowly because the effect of a relatively fast inactivation is unmasked. That is, at small depolarizations, Na$^+$ channel activation in neuroblastoma cells is essentially rate-limiting, indicated by the current reaching peak amplitude at later times after the removal of inactivation (see the Discussion for details).

Fig. 6 shows current traces for a CHOH1 cell at four depolarizations ranging from -60 to -30 mV in the presence and absence of inactivation. Peak currents at each potential are normalized so that peak times can be compared more directly. Note that at all four voltages, currents in the presence and absence of inactivation peak at nearly identical times, indicating that hH1 activation at these small depolarizations is not rate limiting. Similar results were observed many times and were repeated for CHOM1 cells (data not shown), with no change in the time at which the current peaked after the removal of inactivation.

Removal of fast inactivation through mutation has no effect on hH1 activation voltage: papain treatment of hH1Q3 produces a shift in V_a similar to the papain-treated hH1 shift

If rate-limiting activation at small depolarizations were responsible for the measured shift in V_a after the removal of inactivation, then one would predict that any means by which inactivation is removed should cause a shift in V_a. As such, the mutant hH1Q3 (replacing the IFM consensus
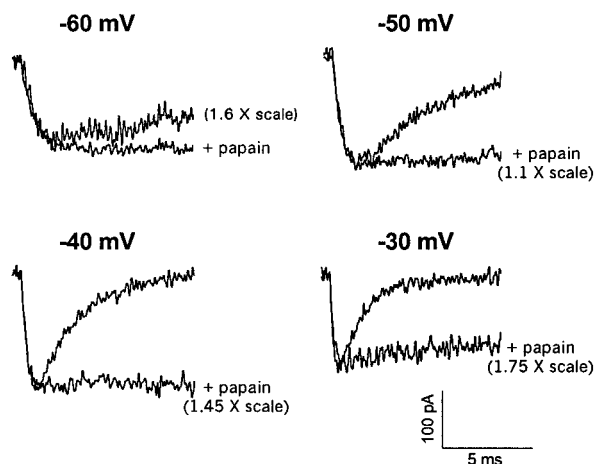
FIGURE 6 Time to peak hH1 current does not change with papain treatment. Whole CHOH1 cell current measured in the presence and absence of inactivation after papain treatment at four small depolarizations. Peak currents at each potential were normalized for comparison. The scaling factor used to normalize is shown beside the adjusted trace. Note that the time at which the currents peak does not change after the removal of inactivation.

inactivation sequence with three glutamine residues to remove fast inactivation; see Hartmann et al., 1994) was transfected into CHO cells, producing essentially noninactivating currents, as shown in Fig. 7 *A*. Fig. 7 *B* shows the *G-V* curve comparing hH1 and hH1Q3, with no significant differences in the voltage dependence of channel activation.

Interestingly, as shown in Fig. 7 *C*, when hH1Q3 is treated with papain, hH1Q3 V_a shifts by nearly 20 mV. This is very similar to the shift in hH1 V_a measured after papain treatment. Thus, as shown in Fig. 7 *B* and *C*, hH1Q3 V_a follows hH1 V_a very closely, both before and after papain treatment. Together, these data directly indicate that the shift in hH1 V_a is not due to the uncoupling of inactivation from activation, but that papain must impose a second, independent effect on hH1 and on hH1Q3.

The III-IV linker may be involved in the shift in hH1 gating

The data shown in Figs. 6 and 7 above indicate that papain has a second, independent effect on hH1 and hH1Q3 activity. In addition to removing inactivation through the apparent clipping of the III-IV linker, it is quite possible that papain also cuts a second loop in hH1 and in hH1Q3 that imposes some structural (or perhaps electrostatic) effect on hH1 activation voltage that is unrelated to inactivation or to the III-IV linker. From the described papain experiments, one can conclude only that some cytoplasmic region of hH1 (hH1Q3) is affected differently than rSkM1 during papain treatment, resulting in a hyperpolarizing shift in hH1 and in hH1Q3 V_a with little or no effect on rSkM1 V_a.

Previously, treatment of rat brain IIA sodium channel with an antibody directed against the conserved III-IV linker region caused a fraction of fast inactivation to be
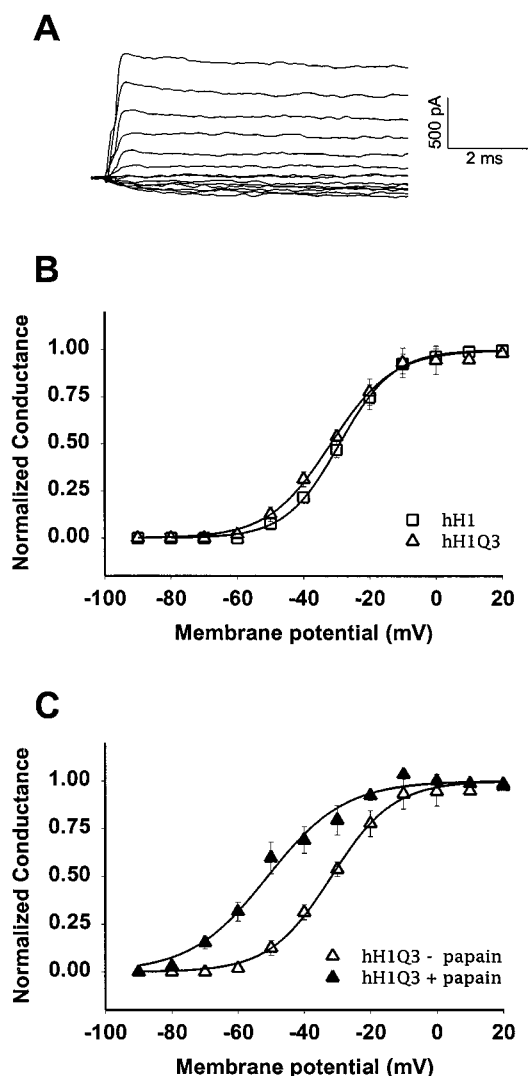

FIGURE 7 Activation voltage of the inactivation-deficient mutant, hH1Q3, closely follows hH1 V_a before and after papain treatment. (*A*) Typical whole-cell Na⁺ current traces from a cell expressing hH1Q3. Currents are measured after a step from the −100 mV holding potential to 10-ms test pulses ranging from −60 through +60 mV in 10-mV steps. (*B*) *G-V* relationship for hH1 versus hH1Q3. Data are the average normalized peak conductance ± SEM at a membrane potential for hH1 (with inactivation intact) versus hH1Q3. Curves are fits of the data to single Boltzmann distributions. □, hH1; $V_a = −28.6 ± 1.8$ mV ($n = 7$). △, hH1Q3; $V_a = −30.8^{\#} ± 2.3$ mV ($n = 4$). (*C*) *G-V* relationship for hH1Q3 before and after papain treatment. Data are the average normalized peak conductance ± SEM at a membrane potential. Curves are fits of the data to single Boltzmann relationships. △, Before papain treatment; $V_a = −30.8 ± 2.3$ mV. ▲, After papain treatment; $V_a = −49.6^{**} ± 3.1$ mV. $n = 4$ for each set.

removed (Vassilev et al., 1988, 1989). As such, an affinity-purified antibody directed against the III-IV region was produced and developed (α1Ab; see Materials and Methods). α1Ab was added to the recording pipette solution to determine whether the III-IV linker region is also responsible for the shift in hH1 V_a.

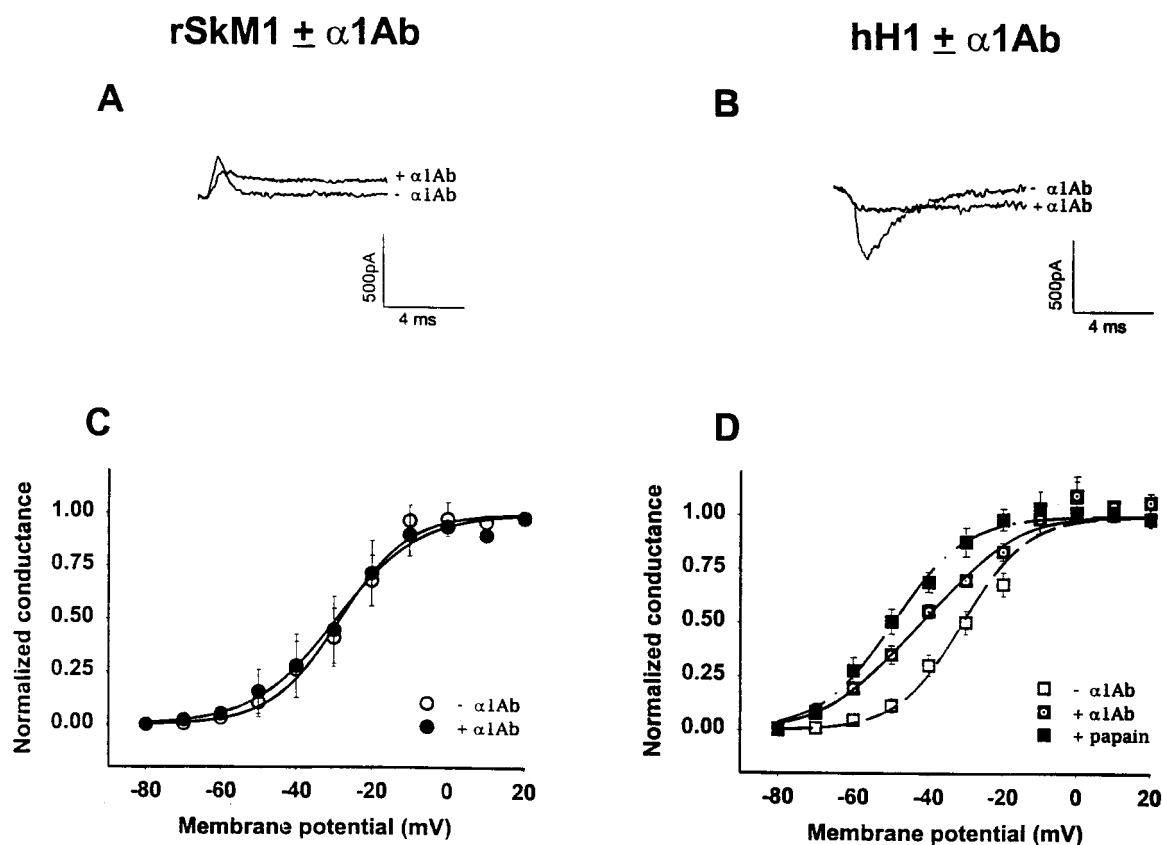Fig. 8, *A* and *B*, gives examples of rSkM1 and hH1 whole-cell currents, respectively, before and after α1Ab

rSkM1 ± α1Ab

A

C

hH1 ± α1Ab

B

D

FIGURE 8 rSkM1 and hH1 inactivation are partially removed through internal perfusion of α1Ab, but only hH1 V_a is shifted. (*A*) Whole-cell current traces from a typical CHOM1 cell to a +30-mV test potential before and after partial removal of inactivation through internal α1Ab treatment. (*B*) Whole-cell current trace from a typical CHOH1 cell to a −30-mV test potential before and after partial removal of inactivation through internal α1Ab treatment. (*C*) *G-V* relationship for rSkM1 before and after α1Ab treatment. Data are the average normalized peak conductance ± SEM at a membrane potential. Curves are fits of the data to single Boltzmann relationships. ○, Inactivation present, $V_a = -28.3 \pm 1.1$ mV. ●, α1Ab treated (averaging 63% inactivation removed), $V_a = -29.3^{\#} \pm 1.1$ mV. $n = 3$ for each set. (*D*) Comparison of *G-V* relationships for hH1 before and after removal of inactivation through papain and α1Ab treatments. Data are the average normalized peak conductance ± SEM at a membrane potential. Nonsolid curves are fits of the data to single Boltzmann relationships. The solid curve represents a fit of the α1Ab-treated hH1 data to a double Boltzmann relationship, fitting 43.7% at −28.74 mV and 56.3% at −52.49 mV. □, Inactivation present; $V_a = -30.2 \pm 2.3$ mV. ■, Inactivation removed through papain treatment; $V_a = -49.3 \pm 2.5$ mV (see Fig. 5 *D*). ⊡, α1Ab treated (averaging 46% inactivation removed), $V_a = -41.9^{**} \pm 1.5$ mV (significance tested against the "inactivation present" data). $n = 7$ for each set.

treatment. For rSkM1, an average 62.8 ± 9.1% of inactivation is removed through α1Ab treatment, ranging from 43% to 82% ($n = 3$). For hH1, antibody treatment removes an average 45.9 ± 4.9% of inactivation, ranging from 20% to 60% ($n = 7$). Fig. 8, *C* and *D*, shows the average *G-V* curves for rSkM1 and hH1, respectively, before and after a 15–30-min exposure to α1Ab. As indicated in Fig. 8 *C*, perfusion of α1Ab in CHOM1 has no effect on rSkM1 V_a, consistent with the papain effects on rSkM1 function. However, as shown in Fig. 8 *D*, hH1 V_a is shifted by ~12 mV with antibody treatment, with the *G-V* relationship for each cell shifted in the hyperpolarized direction.

The antibody effect is epitope-specific

To demonstrate that the effect(s) of α1Ab on hH1 gating is epitope-specific (and not due to some nonspecific effect of

the antibody), α1Ab and the peptide (pep-α1) against which it was made were added together in the intracellular solution. If the effect of α1Ab is epitope-specific, then pep-α1, when added in sufficient amounts, should bind to α1Ab and block the α1Ab effect on channel function. Four cells were tested with the intracellular solution containing both α1Ab and pep-α1, as described in Materials and Methods. The data indicate that α1Ab was effectively blocked by pep-α1 in three of the four cells. That is, current from three of the four cells retained virtually complete inactivation (>90%), indicating that pep-α1 blocked the effect of α1Ab. Fig. 9 *A* shows whole-cell current for a typical CHOH1 cell before and after α1Ab + pep-α1 treatment. Note that pep-α1 protects the channel from any significant removal of inactivation by α1Ab.

Fig. 9 *B* shows the average *G-V* curves for hH1 before and after a 30–40-min perfusion with α1Ab + pep-α1 for the three protected cells. Note that pep-α1, while limiting
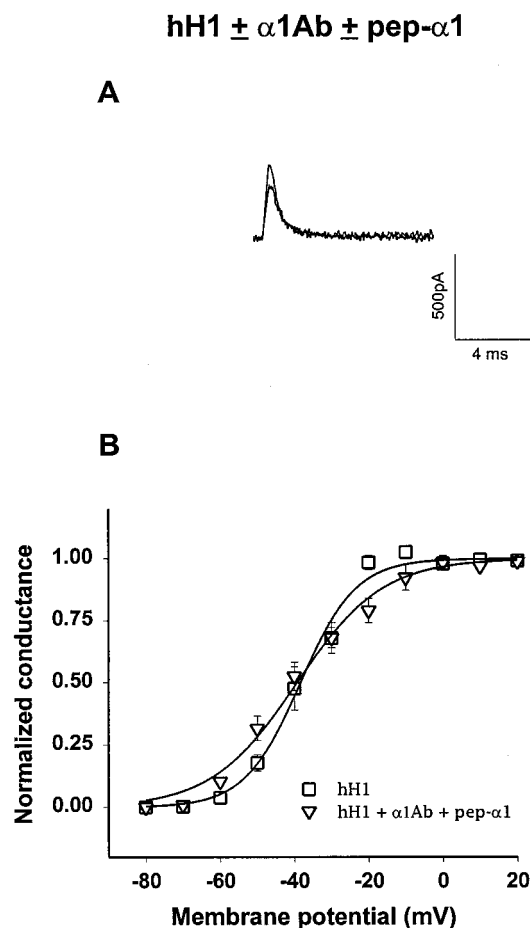
hH1 ± α1Ab ± pep-α1

FIGURE 9   The effect of α1Ab on hH1 V_a is epitope-specific. (*A*) Typical CHOH1 current traces elicited during a +50-mV test potential at 5 and 36 min after WCR. The cell was perfused with 80 μg/ml α1Ab and 80 μg/ml pep-α1. (*B*) *G-V* relationship for hH1 treated with blocked α1Ab. Data are the average normalized conductances ± SEM measured at 5 min ($\square$) and 30–35 min ($\triangledown$) after WCR (*n* = 3). Curves are fits of the data to single Boltzmann relationships.

the removal of inactivation, also prevents the shift in hH1 V_a caused by α1Ab.

For the cell that was not fully protected by pep-α1, 45% of inactivation was removed. In addition, V_a for this cell shifted by 11 mV, similar to the data shown in Fig. 8 *D* for antibody-treated cells. This is consistent, for this lone cell, with pep-α1 effectively not blocking the impact of α1Ab on hH1. For the three protected cells, the data indicate that the effect(s) of α1Ab on hH1 are epitope-specific and thus likely involve regions within or intimate with the III-IV linker.

DISCUSSION

Through direct comparison of the adult skeletal muscle (rSkM1) versus cardiac and embryonic skeletal muscle (hH1) sodium channel isoforms, one can begin to characterize differences in sodium channel activity expressed dur-

ing distinct developmental stages and in various adult non-neuronal excitable tissues. rSkM1 and hH1 were expressed in CHO cells, and steady-state and kinetic voltage-dependent gating behaviors were compared. In general, rSkM1 gates at more depolarized potentials than hH1, with V_a 7 mV and V_i 10 mV more depolarized for rSkM1 than for hH1. Consistent with the relative potential dependence of the steady-state parameters, hH1 gates more rapidly than rSkM1 at most tested potentials. Furthermore, rSkM1 recovers from inactivation faster than hH1 (a 1-ms versus 2-ms time constant at a −120-mV recovery potential), while the potential dependencies of recovery for the two isoforms were similar.

Thus some basic but relatively subtle differences between rSkM1 and hH1 function as expressed in CHO cells are observed. Some of these functional differences between isoforms are distinct from those previously reported for rSkM1 and hH1 function as transiently expressed in tsA201 cells (Chahine et al., 1996). These include smaller differences in V_a and V_i, and in inactivation rates. This probably indicates a functional impact of the cellular system on channel activity and serves as a reminder of the limitations of heterologous expression systems. However, because whole-cell recordings of sodium channels expressed in CHO cells show no indication of a time-dependent shift in V_a, CHO cells provide a good cellular system for studying sodium channel activity, particularly voltage- and time-dependent mechanisms.

Together, the more rapid activation and inactivation kinetics and the slower times to recovery from inactivation for hH1 compared with rSkM1 are consistent with hH1 designed for more rapid progress into the active and inactive states, while rSkM1 will tend to spend more time in the closed state.

Internal treatment with papain or with α1Ab causes a hyperpolarizing shift in hH1 V_a but not rSkM1 V_a

Cytoplasmic treatment with a protease or with a site-directed antibody revealed a significant functional difference between rSkM1 and hH1. As shown in Fig. 5, hH1 V_a shifts significantly after papain treatment, while rSkM1 V_a is insignificantly altered. Treatment with an affinity-purified antibody directed against the conserved III-IV linker region, α1Ab, partially removed inactivation of both hH1 and rSkM1 (removing an average 46% and 63% inactivation, respectively). Only hH1 V_a was affected, shifting by ~12 mV after a 20–30-min antibody treatment, with an insignificant 1-mV effect on rSkM1 V_a. Furthermore, the effect of α1Ab was shown to be epitope-specific, as illustrated in Fig. 9, with the effect of α1Ab blocked through coperfusion of pep-α1. Together, the data reveal a significant difference between hH1 and rSkM1 activation mechanisms.

What causes a shift in hH1 activation voltage but not in rSkM1 activation voltage?

Is the shift in hH1 V_a coupled to the removal of inactivation, or is the shift caused by some other phenomenon, such as a time-dependent shift in V_a or a second, independent effect of papain and α1Ab on hH1 activation voltage? Fig. 1 directly demonstrates that neither hH1 nor rSkM1 activation voltages "drift" over time, and thus a time-dependent shift in V_a cannot explain the 20-mV shift in hH1 V_a that was measured after the removal of inactivation (over time). Second, care was taken to ensure that all data measured were corrected for series resistance (95–98%). To limit further the impact of any series resistance error, experiments were done using set B solutions as described in Materials and Methods. These solutions produce lower currents, further minimizing any residual series resistance effect on voltage. Thus the impact of series resistance on the measured V_a is minimal (<1 mV) and cannot account for a 20-mV shift in V_a.

The kinetic uncoupling of inactivation from slow activation cannot account for the shift in hH1 activation voltage

As described in the Results, Gonoi and Hille (1987) elegantly showed that a 25-mV shift in neuroblastoma sodium channel V_a was due to the uncoupling of fast inactivation from a slow activation at small depolarizations. The following discussion illustrates that activity of hH1 in CHO cells cannot be explained by the neuroblastoma model, suggesting that the shifts in hH1 V_a caused by papain and α1Ab treatments are not due to a kinetic uncoupling of inactivation from activation. The predictions of the neuroblastoma model are presented, followed by an explanation of how the data do not support the predictions:

1. The neuroblastoma model predicts that currents at small depolarizations will reach peak magnitude at a later time after the removal of inactivation. When inactivation is present, the current at small depolarizations will reach peak magnitude more quickly because of the coincidence of slow activation with fast inactivation. The percentage of channels in the inactive state at the time of peak current will be greater at smaller depolarizations, decreasing with depolarization because of the increase in activation rates with depolarization. The resulting change in the relative distribution of channels among states with depolarization results in a measured shift in V_a (see Hille, 1992, for details). When inactivation is removed, activation can continue unimpeded by inactivation, and the current will reach its true peak value, albeit at a later time. As illustrated in Figs. 6 and 8 B, there is no change in the time at which hH1 currents peak at any potential after the removal of inactivation.

2. The neuroblastoma model predicts that V_a is artificially depolarized in the presence of inactivation. Removing inactivation through any means should unmask this depolarizing shift, resulting in the measurement of a more hyperpolarized V_a. Fig. 7 directly shows that removal of inactivation through mutation has no effect on channel activation voltage, and thus the unmasking of a rate-limiting (or at least slow) activation after the removal of inactivation cannot account for the 20-mV shift in hH1 V_a.

A structural difference between rSkM1 and hH1 that is linked somehow to the III-IV linker may explain the observed functional diversity

While the neuroblastoma model describes sodium channel activity in neuroblastoma cell lines, the data presented here indicate directly that the 12–20-mV shift in hH1 V_a measured after antibody and papain treatment cannot be explained by this model. Papain and antibody treatments similarly remove inactivation from rSkM1 and from hH1. However, a second phenomenon, a shift in hH1 V_a while rSkM1 V_a remains nearly constant, appears to be independent of the removal of inactivation. As shown in Fig. 7, activation voltage for the inactivation-deficient mutant, hH1Q3, is nearly identical to hH1 V_a both before and after papain treatment, with hH1 and hH1Q3 shifting by ~20 mV in the hyperpolarized direction after papain treatment. These data indicate that the shift in hH1 V_a is not due to the uncoupling of inactivation from activation, but that papain (α1Ab) has a second, independent effect on hH1 that is not observed for papain (α1Ab)-treated rSkM1.

Thus the data suggest that there is a functionally important cytoplasmic (or a structure that is linked to cytoplasmic regions) structural difference between rSkM1 and hH1. This structure somehow alters the voltage dependence of hH1 activation, but not rSkM1 activation, and is apparently localized either to the III-IV linker or to an area interacting with this region (see Fig. 8). Papain and α1Ab treatment alter the impact this structure has on channel function, causing a measured shift in hH1 V_a.

These data are the first to describe a phenomenon in which channel cytoplasmic regions impact the voltage dependence of cardiac channel activation. While several studies have implicated S4 segments involved in the inactivation mechanism of the channel (Chen et al., 1996; Ji et al., 1996; Cha et al., 1999), cytoplasmic effects on cardiac channel activation mechanisms have not been described.

Through the parallel functional comparison of two sodium channel isoforms, a significant difference in channel function was observed. The data are consistent with a cytoplasmic structure within, near, or interacting with the III-IV linker of hH1 that alters the voltage dependence of channel activation. This structure helps to set hH1 activation voltage to more depolarized potentials. Disrupting or interacting with this region allows the channel to activate at lesser depolarizations and thus causes a shift in hH1 V_a. There cannot be complete overlap of this region and the consensus inactivation sequence (IFM), given the data showing that hH1Q3 V_a and wild-type hH1 V_a are affected similarly by papain. Moreover, given the similarities between hH1 and rSkM1 III-IV linker regions (only seven of

the 53 amino acids making up the III-IV linker regions differ between the two isoforms), other regions with which the III-IV linker is involved may be responsible for the observed shift in hH1 V_a. Because rSkM1 V_a did not shift after papain or α1Ab treatment, rSkM1 is either missing this region, or this region is differently linked (if at all) to channel activation. Comparative studies of structural differences between hH1 and rSkM1 within, near, or involved with the III-IV linker would be informative and are necessary to gain insight into the specific region(s) responsible for this phenomenon.

REFERENCES

Armstrong, C. M., and F. Bezanilla. 1973. Destruction of sodium conductance inactivation in squid axons perfused with pronase. *J. Gen. Physiol.* 62:375–391.

Armstrong, C. M., and F. Bezanilla. 1977. Inactivation of the sodium channel. II. Gating current experiments. *J. Gen. Physiol.* 70:567–590.

Bennett, E., M. S. Urcan, S. S. Tinkle, A. G. Koszowski, and S. R. Levinson. 1997. Contribution of sialic acid to the voltage dependence of sodium channel gating: a possible electrostatic mechanism. *J. Gen. Physiol.* 109:327–343.

Catterall, W. A. 1995. Structure and function of voltage-gated ion channels. *Annu. Rev. Biochem.* 64:493–531.

Cha, A., P. C. Ruben, A. L. George, Jr., E. Fujimoto, and F. Bezanilla. 1999. Voltage sensors in domains III and IV, but not in I and II, are immobilized by Na$^+$ channel fast inactivation. *Neuron.* 22:73–87.

Chahine, M., I. Deschene, L.-Q. Chen, and R. G. Kallen. 1996. Electrophysiological characteristics of cloned skeletal and cardiac muscle sodium channels. *Am. J. Physiol.* 271:H498–H506.

Chen, L.-Q., M. Chahine, R. G. Kallen, R. L. Barchi, and R. Horn. 1992. Chimeric study of sodium channels from rat skeletal and cardiac muscle. *FEBS. Lett.* 309:253–257.

Chen, L.-Q., V. Santarelli, R. Horn, and R. G. Kallen. 1996. A unique role for the S4 segment of domain 4 in the inactivation of sodium channels. *J. Gen. Physiol.* 108:549–556.

Eaton, D. C., M. S. Brodwick, G. S. Oxford, and B. Rudy. 1978. Arginine-specific reagents remove sodium channel inactivation. *Nature.* 271: 473–476.

Gellens, M. E., A. L. George, Jr., L. Chen, M. Chahine, R. Horn, R. L. Barchi, and R. G. Kallen. 1992. Primary structure and functional expression of the human cardiac tetrodotoxin-insensitive voltage-dependent sodium channel. *Proc. Natl. Acad. Sci. USA.* 89:554–558.

Gonoi, T., and B. Hille. 1987. Gating of Na$^+$ channels. Inactivation modifiers discriminate among models. *J. Gen. Physiol.* 89:253–273.

Harlow, E., and D. Lane. 1988. Storing and purifying antibodies. *In* Antibodies: A Laboratory Manual. Cold Spring Harbor Laboratory, Cold Spring Harbor, NY. 310.

Hartmann, H. A., A. A. Tiedeman, S.-F. Chen, A. M. Brown, and G. E. Kirsch. 1994. Effects of III-IV linker mutations on human heart Na$^+$ channel inactivation gating. *Circ. Res.* 75:114–122.

Hille, B. 1992. Ion Channel of Excitable Membranes, 2nd Ed. Sinauer Associates, Sunderland, MA. 446–449, 494–501.

Horn, R., M. S. Brodwick, and D. C. Eaton. 1980. Effect of protein cross-linking reagents on membrane currents of squid axon. *Am. J. Physiol.* 238:C127–C132.

Jan, L. Y., and Y. N. Jan. 1997. Cloned potassium channels from eukaryotes and prokaryotes. *Annu. Rev. Neurosci.* 20:91–123.

Ji, S., A. L. George, Jr., R. Horn, and R. L. Barchi. 1996. Paramyotonia congenita mutations reveal different roles for segments S3 and S4 of domain D4 in hSkM1 sodium channel gating. *J. Gen. Physiol.* 107: 183–194.

Kallen, R. G., S. A. Cohen, and R. L. Barchi. 1993. Structure, function and expression of voltage-dependent sodium channels. *Mol. Neurobiol.* 7:383–428.

Keynes, R. D. 1986. Modeling the sodium channel. *In* Ion Channels in Neural Membranes: Proceedings of the 11 International Conference on Biological Membranes. J. Ritchie, R. D. Keynes, and L. Bolis, editors. Liss, New York. 86–101.

Kirsch, G. E., A. Skattebol, L. D. Possani, and A. M. Brown. 1989. Modification of Na channel gating by an α scorpion toxin from *Tityus serrulatus. J. Gen. Physiol.* 93:67–83.

Oxford, G. S. 1981. Some kinetic and steady-state properties of sodium channels after removal of inactivation. *J. Gen. Physiol.* 77:1–22.

Oxford, G. S., C. H. Wu, and T. Narahashi. 1978. Removal of sodium channel inactivation in squid axons by *N*-bromoacetamide. *J. Gen. Physiol.* 71:227–247.

Patlak, J. 1991. Molecular kinetics of voltage-dependent Na$^+$ Channels. *Physiol. Rev.* 71:1047–1080.

Richmond, J. E., D. E. Featherstone, H. A. Hartmann, and P. C. Ruben. 1998. Slow inactivation in human cardiac sodium channels. *Biophys. J.* 74:2945–2952.

Rogart, R. B., L. L. Cribbs, L. K. Muglia, D. D. Kephart, and M. W. Kaiser. 1990. Functional properties of rat brain sodium channels expressed in a somatic line. *Science.* 247:854–858.

Stimers, J. R., F. Bezanilla, and R. E. Taylor. 1985. Sodium channel activation in the squid giant axon. Steady state properties. *J. Gen. Physiol.* 65:65–82.

Stuhmer, W., F. Conti, H. Suzuki, X. Wang, M. Noda, N. Yahagi, H. Kubo, and S. Numa. 1989. Structural parts involved in activation and inactivation of the sodium channel. *Nature.* 339:597–603.

Trimmer, J. S., S. S. Cooperman, W. S. Agnew, and G. Mandel. 1990. Regulation of muscle sodium channel transcripts during development and in response to denervation. *Dev. Biol.* 142:360–367.

Trimmer, J. S., S. S. Cooperman, S. A. Tomiko, J. Zhou, S. M. Crean, M. B. Boyle, R. G. Kallen, Z. Sheng, R. L. Barchi, F. J. Sigworth, R. H. Goodman, W. S. Agnew, and G. Mandel. 1989. Primary structure and functional expression of a mammalian skeletal muscle sodium channel. *Neuron.* 3:33–49.

Ukomadu, C., J. Zhou, F. J. Sigworth, and W. S. Agnew. 1992. μ1 Na$^+$ channels expressed transiently in human embryonic kidney cells: biochemical and biophysical properties. *Neuron.* 8:663–676.

Vassilev, P. M., T. Scheuer, and W. A. Catterall. 1988. Identification of an intracellular peptide segment involved in sodium channel inactivation. *Science.* 241:1658–1664.

Vassilev, P., T. Scheuer, and W. A. Catterall. 1989. Inhibition of inactivation of single sodium channels by a site-directed antibody. *Proc. Natl. Acad. Sci. USA.* 86:8147–8151.

Wang, D. W., A. L. George, Jr., and P. B. Bennett. 1996. Comparison of heterologously expressed human cardiac and skeletal muscle sodium channel. *Biophys. J.* 70:238–245.

West, J. W., T. Scheuer, L. Maechler, and W. A. Catterall. 1992. Efficient expression of rat brain type IIA Na$^+$ channel α subunits in a somatic cell line. *Neuron.* 8:59–70.

Yang, J., J. T. Sladky, R. G. Kallen, and R. L. Barchi. 1991. TTX-sensitive and TTX-Insensitive sodium channel mRNA transcripts are independently regulated in adult skeletal muscle after denervation. *Neuron.* 7:421–427.